PHILOSOPHICAL TRANSACTIONS OF THE ROYAL SOCIETY A MATHEMATICAL, PHYSICAL & ENGINEERING SCIENCES

ICE Observations of Comet Giacobini-Zinner

S. W. H. Cowley

Phil. Trans. R. Soc. Lond. A 1987 **323**, 405-420
doi: 10.1098/rsta.1987.0095

Phil. Trans. R. Soc. Lond. A **323**, 405–420 (1987)
Printed in Great Britain

ICE observations of Comet Giacobini-Zinner

By S. W. H. Cowley
Blackett Laboratory, Imperial College, London SW7 2BZ, U.K.

The first spacecraft encounter with a comet took place on 11 September 1985 when the International Cometary Explorer spacecraft passed through the tail of Comet Giacobini-Zinner at a distance of 7800 km from the nucleus. It provided the first definitive *in-situ* information concerning the interaction of a cometary atmosphere with the flowing solar-wind plasma, and the results of initial analyses are reviewed in this paper. Large-scale MHD aspects of the interaction largely conform to prior expectation. The flow surrounding the comet is mass-loaded and slowed by *in situ* ionization and pick-up of heavy cometary neutrals, and the solar-wind magnetic field consequently becomes draped around the obstacle, and forms an induced magneto-tail. Substantial evidence exists for the permanent presence of a weak shock lying in the subsolar mass-loaded region upstream from the comet, through whether the spacecraft itself passed through shocks on the cometary flanks remains controversial. There is no doubt, however, that a sharp boundary was observed both inbound and outbound (centred on *ca.* 09h29 and 12h20 U.T.) whose width is an energetic heavy-ion Larmor radius (*ca.* 10^4 km), where the flow is deflected away from the comet and slowed, and where the magnetic field and plasma become compressed and very turbulent. The location of this boundary is also consistent with that expected for a weak shock based upon the known Giacobini-Zinner water-molecule production rate. An unexpected feature of the interaction was the extreme levels of field and plasma turbulence, and broadband wave activity observed in the region of mass-loaded flow.

1. Introduction

On 11 September 1985 the first ever close encounter took place between a spacecraft and a comet when the International Cometary Explorer (ICE) spacecraft passed through the tail of Comet Giacobini-Zinner at a distance of 7800 km from its central nucleus. The results of initial analyses of the ICE data have recently been published, and in this paper we will present a brief overview. The ICE spacecraft was not specifically designed for cometary studies. In particular it carried no cameras or instruments to investigate the comet's neutral atmosphere, and only rudimentary measurements of the dust were possible. Rather, the spacecraft's prime mission following launch in August 1978 was to study plasma particles and electromagnetic fields in the solar wind upstream from the Earth's magnetosphere as part of the NASA–ESA International Sun–Earth Explorer programme. Consequently, the data returned by ICE from Giacobini-Zinner concern plasmas and fields in its vicinity, and relates principally to the interaction between the comet's atmosphere and the flowing solar-wind plasma.

The nature of this interaction is quite different from that between the solar wind and planetary bodies in the Solar System (see, for example, Mendis & Houpis 1982). When the cometary nucleus approaches the Sun, the ices of which it is composed (mainly water) sublime, and being unrestrained by gravity, the resulting gases expand away at speeds of *ca.* 1 km s^{-1}

producing an extensive neutral atmosphere or coma. Water molecules in the coma are photodissociated by sunlight on time scales of *ca.* 10^5 s (at *ca.* 1 AU), so that at distances exceeding a few hundred thousand kilometres the coma becomes dominated by atomic oxygen and hydrogen. Being highly tenuous and nearly collision-free, the solar wind blows continuously through this coma, and there is little interaction between the two populations. However, on timescales of a few million seconds (and hence on spatial scales of a few million kilometres surrounding the nucleus) the atoms in the coma become ionized, either by solar UV radiation or by charge exchange with solar-wind protons. The ions are then 'picked up' by the flow, moving in cycloidal orbits in the crossed electric and magnetic fields of the solar wind. As the 'pick-up' ions gyrate about the magnetic field, their energy in the comet frame (spacecraft frame) varies between essentially zero and a maximum energy,

$$E_{\max} = 4\,A \sin^2 \alpha E_{\mathrm{sw}}. \tag{1}$$

where A is the ion mass in unified atomic mass units, α is the cone angle between the magnetic field and the velocity vector in the solar wind and E_{sw} is the energy of a proton moving at the solar-wind speed. For typical wind speeds of *ca.* 450 km s^{-1} solar-wind protons have an energy $E_{\mathrm{sw}} \approx 1$ keV, so that 'pick-up' protons have energies extending to *ca.* 4 keV, and 'pick-up' oxygen is energized up to *ca.* 64 keV (for $\sin^2 \alpha = 1$). Thus heavy particles, particularly, gain large energies from the pick-up process. This energy is extracted from the solar-wind flow, such that sufficiently close to the comet where the mass density of the pick-up ions starts to become a sensible fraction of the solar-wind mass density, the flow becomes 'mass-loaded' and slowed. Theory (see, for example, Ip & Axford 1982) suggests that a weak shock should lie near the periphery of the mass-loaded region, where the heavy ions first reach *ca.* 1% of the solar wind by number density. At the time of the ICE encounter the Giacobini-Zinner water production rate was *ca.* (2–3) $\times$ 10^{28} molecules s^{-1} (Combi *et al.* 1986; Strauss *et al.* 1986), leading to estimates of the spatial scale of the mass-loaded region of *ca.* 10^5 km. As the impinging flow slows, the frozen-in magnetic field becomes distorted and 'draped' around the central region as first proposed by Alfvén (1957), and as depicted schematically in figure 1. Most of the plasma flow and embedded field slips 'around' the central region, out of the plane of the diagram, but some flux tubes can become 'captured' near to the nucleus by mass-loading, perhaps for intervals of 1 h or more. Because the 'ends' of these field lines remain frozen to the flowing solar-wind plasma away from the comet, these 'captured' flux tubes become stretched out on the antisolar side of the comet to form an induced magnetotail. The form of the tail should be approximately cylindrical, bisected by a current sheet separating fields of opposite polarity (figure 1). Cold cometary plasma flowing along these 'captured' flux tubes then gives rise to the visible 'ion' (type 1) comet tails.

Figure 1 also shows the trajectory of ICE relative to the comet structure. Giacobini-Zinner is a short-period (6.5 years) comet, which moves in a prograde orbit inclined at 31.9° to the ecliptic between the orbits of Jupiter and the Earth (perihelion 1.03 AU). At the time of the encounter the comet was 6 d past perihelion, moving from north to south across the ecliptic plane with little radial component of velocity. Fortuitously, the azimuthal component of the comet velocity nearly matched that of the spacecraft (*ca.* 30 km s^{-1}), such that relative to the comet, ICE passed very nearly directly south to north through the comet structure at a speed of *ca.* 21 km s^{-1}. ICE was targeted to the antisolar side of the comet, and passed centrally through the ion tail with an impact parameter of 7800 km relative to the nucleus

PHILOSOPHICAL TRANSACTIONS OF THE ROYAL SOCIETY A MATHEMATICAL, PHYSICAL & ENGINEERING SCIENCES

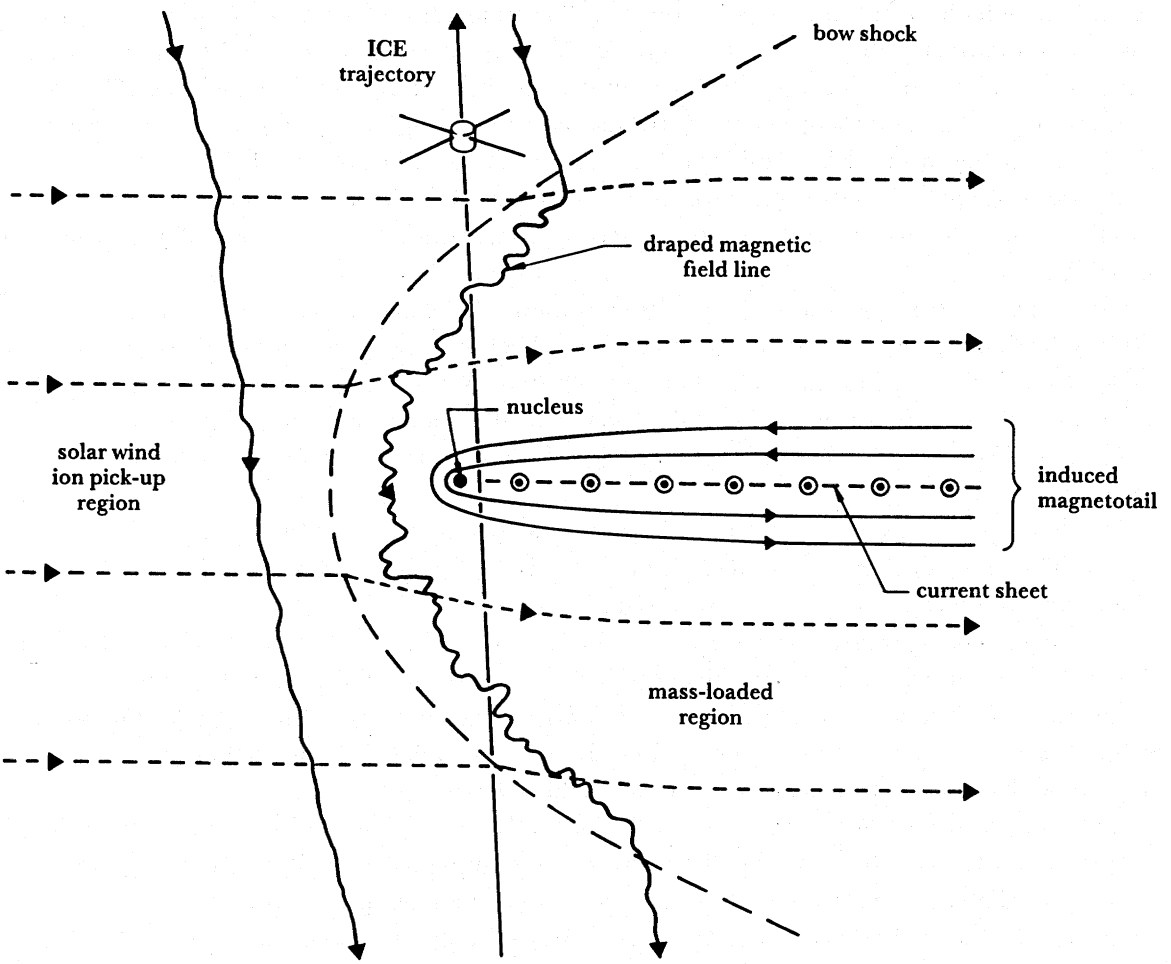

FIGURE 1. Sketch showing the main theoretically expected features of the interaction between the atmosphere of Comet Giacobini-Zinner and the solar-wind plasma, together with the trajectory of the ICE spacecraft relative to those regions. Solid arrowed lines show magnetic field lines, short-dashed arrowed lines are plasma streamlines, and the long-dashed line is the bow shock, lying in the outer part of the region of slowed, mass-loaded flow.

(von Rosenvinge *et al.* 1986). It should be noted for purposes of later discussion that with this relative trajectory the principal signatures of field-draping should depend upon the sign of the north–south component of the solar-wind magnetic field, because the spacecraft would fly approximately along the current sheet for a purely east–west field. For a southerly directed field as depicted in figure 1, the draped field should be deflected antisunward to the south of the comet (inbound) and sunward to the north of the comet (outbound), and vice versa for a northward-directed field.

The spatial scales discussed above can now be translated to timescales on the ICE trajectory, there being three basic regions of interest. First, an 'ion pick-up region' should extend a few million kilometres from the comet, where significant heavy-ion 'pick-up' fluxes should be present in the solar wind, but where densities remain sufficiently small that the flow is not affected. At *ca.* 20 km s^{-1} this translates to plus or minus a few days on the spacecraft trajectory about closest approach. Second, the 'mass-loaded region' with slowed flows has a scale of

ca. 10^5 km which translates to ± 1 hour on the trajectory. Third, telescopic observations indicate the radius of the cold ion tail to be *ca.* 10^4 km, corresponding to ± 10 min on the ICE trajectory. (The central current sheet presents a smaller interior scale, which, as ICE observations show, has a dimension of *ca.* 10^3 km corresponding to ± 1 min). These timescales should be borne in mind in considering the ICE data in the sections below.

Before turning to the latter, however, we first itemize the relevant ICE instrumentation and briefly summarize its capabilities (the associated institution given is that of the principal investigator).

(*a*) *Plasma electron spectrometer* (*Los Alamos National Laboratory*). Covered the energy range 10–1000 eV and provided one 3 s two-dimensional ecliptic azimuth–energy distribution every 24 s. Moment integrations then yield the electron density and temperature, n_e and T_e, together with the ecliptic plane projections of the electron bulk velocity and heat flux.

(*b*) *Magnetometer* (*Jet Propulsion Laboratory*). Provided three magnetic field vectors per second.

(*c*) *Plasma-wave experiment* (*TRW*). Measured electric fields from 18 Hz to 100 kHz (90 m tip-to-tip dipole) and magnetic fields from 0.32 Hz to 1 kHz (search coil). Detected plasma waves and impulsive noise from dust impacts.

(*d*) *Radio-wave experiment* (*Observatoire de Paris*). Measured electric fields from 30 kHz to 2 MHz. Determined n_e, T_e (for sufficiently large n_e) from thermal-plasma emission.

(*e*) *Energetic-ion detector* (*ULECA*) (*Max-Planck-Institut, Garching*). Obtained two-dimensional ecliptic azimuth–energy distributions of ions from 35 to 150 keV. Measured energetic pick-up ions, though response to heavy ions is of low efficiency.

(*f*) *Energetic-ion detector* (*EPAS*) (*Imperial College, London*). Measured one three-dimensional ecliptic azimuth–elevation–energy distribution of pick-up ions every 32 s. The energy range is mass-dependent; 65 keV to several mega electron volts for water-group ions.

(*g*) *Ion-composition experiment* (*Goddard Space Flight Center*). Measured ions of mass 1.4–3 u in the speed range 237–463 km s^{-1} (appropriate to solar-wind alphas) and ions of mass 14–33 u in the range 80–223 km s^{-1} (appropriate to heavy cometary ions in the slowed mass-loaded region). Long instrument cycle time of 21.1 min.

The major gap in the above list (as regards plasma physics) is the lack of thermal-ion data of high temporal resolution.

The next sections will now describe in turn the main results obtained by this instrumentation concerning the thermal plasma, magnetic field, plasma waves and energetic heavy ions.

2. Thermal-plasma observations

Figure 2 gives an overview of the encounter data obtained by the electron spectrometer (Bame *et al.* 1986). Data for 10 h are shown, with closest approach occurring at 11h03 min 38 s U.T., nearly at the centre of the diagram. The panels display the electron density n_e, temperature T_e and ecliptic plane projection of the bulk speed V_e, and clearly show the presence of three basic regions, though these have been further subdivided by Bame *et al.* (1986) in the panel above the data. At the beginning and end of the interval the spacecraft is located in the solar wind (sw), though effects of heavy-ion pick up are clearly present as will be outlined below. The mass-loaded region where the plasma speed is substantially reduced by pick up is then traversed between *ca.* 09h20 and 12h20 U.T. (marked TR and S), corresponding to

PHILOSOPHICAL TRANSACTIONS OF THE ROYAL SOCIETY A MATHEMATICAL, PHYSICAL & ENGINEERING SCIENCES

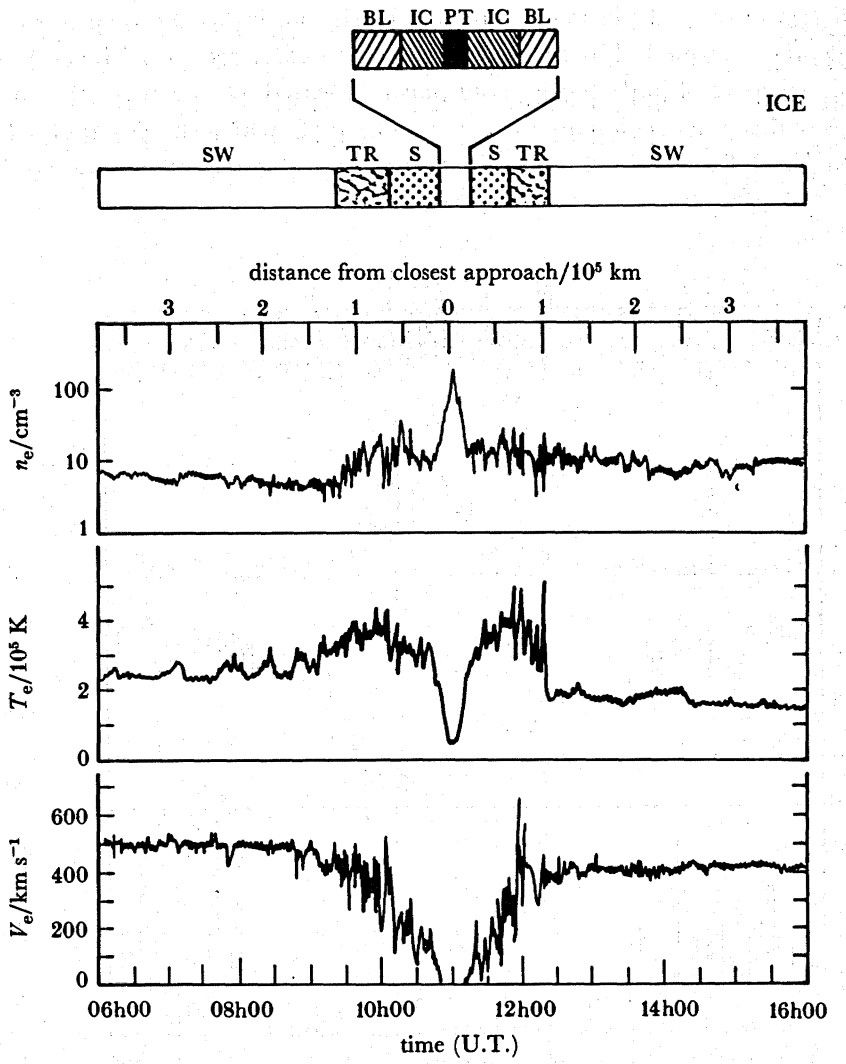

FIGURE 2. Overview of the electron density, temperature and ecliptic plane bulk speed observed by the electron spectrometer during the Giacobini-Zinner encounter. Three-point running averages are shown. The key at the top of the plot identifies the plasma regions encountered, as follows: SW, solar wind; TR, transition region; S, sheath; BL, boundary layer; IC, intermediate coma; PT, plasma tail. (From Bame *et al.* 1986.)

distances of $\pm 10^5$ km about closest approach as indicated by the scale at the top of the diagram, and in the discussion of the preceding section. (It may be noted, however, that small depressions in flow speed are clearly evident for at least 30 min outside the times indicated.) This region is further subdivided by Bame *et al.* (1986) into an outer transition region (TR) and inner sheath (S) for reasons described further below. All of these regions are characterized by flow that is predominantly antisolar (see, for example, Baker *et al.* 1986), and plasma that has at least a significant solar-wind component. In the central 25 min of the encounter, however, ICE entered a region believed to be dominated by dense, cold cometary plasma where the flow speed is smaller than can be detected by this instrument (not more than about 30 km s^{-1}). This region, of width *ca.* 3×10^4 km, is separated from the sheath by a boundary layer (BL) of intermediate characteristics believed to have the nature of a diffuse contact surface, interior to

which there is a region of cold plasma where the density varies as the inverse square of the distance to the comet (termed the 'intermediate coma' (IC); see also Meyer-Vernet *et al.* 1986*b*) with a sharp spike of high density cold plasma located at its centre (the 'plasma tail' (PT)). The details of this inner region are displayed in figure 3, which shows data for 1 h centred on closest approach in a format similar to figure 2. The high-density spike is observed for 3 min

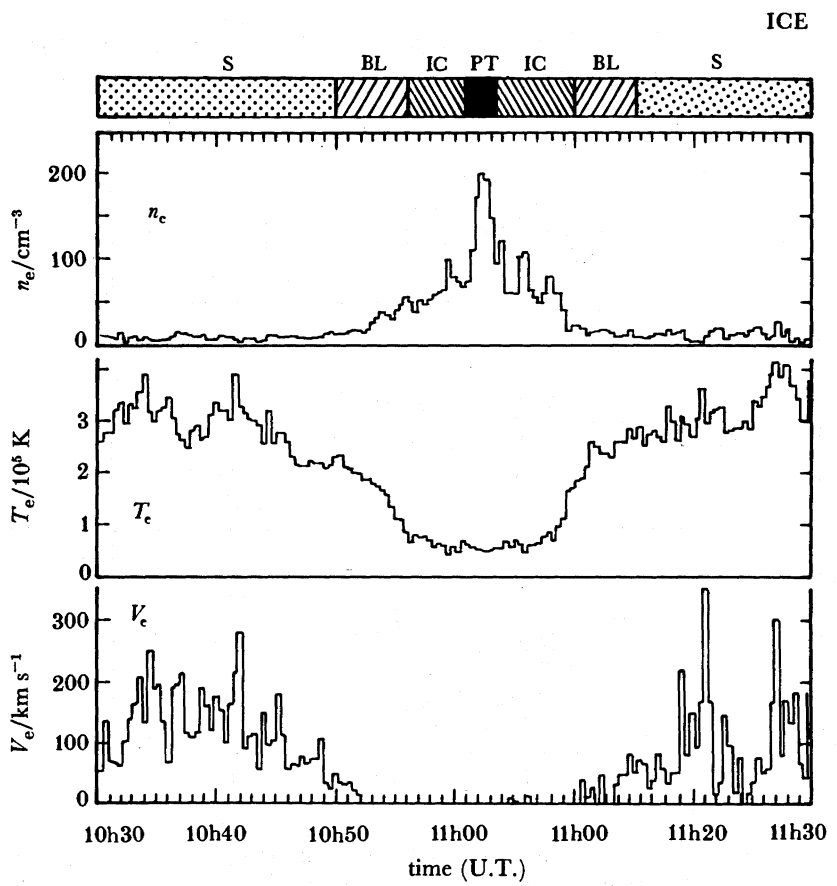

FIGURE 3. Expanded plot of the region nearest closest approach in the same format as figure 2, except that the data are here unsmoothed. (From Bame *et al.* 1986.)

at the spacecraft, corresponding to a width of 3000 km, though the highest density and coldest plasma (*ca.* 650 cm^{-3} and *ca.* 1 eV (Meyer-Vernet *et al.* (1986 *a*, *b*)) is observed for only *ca.* 1 min, or *ca.* 1200 km along the spacecraft track. In the next section it will be shown that an induced magnetotail is contained within the 'intermediate coma' region, and that the 'spike' in fact corresponds to a crossing of the central current sheet.

We now discuss further details of the plasma observations, taking each of the three main regions in turn. The major feature of the solar wind surrounding the comet is the presence of fluctuations in the electron density and temperature (generally anticorrelated) with characteristic timescales of *ca.* 2 min (Bame *et al.* 1986; Gosling *et al.* 1986). Convected at a solar-wind speed of *ca.* 500 km s^{-1}, this time corresponds to a spatial scale of *ca.* 6×10^4 km. These fluctuations are undoubtedly due to an electromagnetic instability set up by the pick-up process

(see next section). They were first observed at distances of *ca.* 10^6 km from the comet, the amplitude increasing as the comet was approached and peaking with $\delta n/n \approx 1$ in the 'transition region', before falling slightly in amplitude in the 'sheath'. Thus, in agreement with the previous section, these results indicate that ion pick up takes place in a region at least *ca.* 10^6 km in extent. The largest density spikes in the 'transition region' have $\delta n/n \approx 3$–5, and are accompanied by large perturbations in the flow speed and direction, though no systematic pattern has been found (Baker *et al.* 1986). Evidence also exists that these large density fluctuations occur not only in the mass-loaded region along the north–south trajectory of the spacecraft, but also along similar path lengths (*ca.* 10^5 km) in the transverse spacecraft–Earth direction. This has been deduced by Steinberg *et al.* (1986) from analysis of the angular broadening of the Earth radio source (kilometric waves from the auroral zone) observed during encounter by the ICE radio-wave experiment.

Turning now to the mass-loaded region, it can be seen that although the plasma is compressed, heated and slowed as it passes from the solar wind into the transition region it is not possible in the presence of the large fluctuations to convincingly identify a single weak shock structure. Nevertheless, sharp features do occur in the density and temperature data, particularly in T_e at *ca.* 12h20 U.T. Within the 'sheath' region the electron spectra also consistently show evidence that the particles have passed through a weak shock (Thomsen *et al.* 1986). In the solar wind the spectra are of the usual two-component form with a thermal 'core' of 20 eV and a high-energy tail or 'halo' above *ca.* 100 eV. In the 'sheath' the latter population remains relatively constant in form (at least above *ca.* 300 eV), while the core becomes heated and 'flattened', indicative of the effect of the shock potential. Thomsen *et al.* infer that the sheath streamlines pass through a weak shock that is a permanent feature of the subsolar mass-loading region. In the transition region, however, they report variable spectra that are sometimes sheath-like and sometimes solar-wind-like (though heated), and infer that a shock is present only intermittently on the flanks, possibly as a result of the strong fluctuations present in the inflow plasma, as described above. In particular, they infer that no shock was actually crossed by the spacecraft on its north–south trajectory, although this topic will be taken up again later.

The electrons in the high-energy tail of the distribution of the heated plasma in the mass-loaded region escape continuously into the upstream region by flow along the magnetic field lines. When ICE was in the solar wind and magnetically connected to the mass-loaded region it detected this as an approximately sunward-directed field-aligned heat flux of electrons with energies of more than 100 eV. These heat-flux events were observed at distances of up to *ca.* 5×10^5 km from the comet (giving rise to the sporadic enhancements of T_e seen in the solar wind in figure 2, particularly during the inbound pass), and are important in allowing one to sense remotely the shape of the hot-particle source, because the magnetic field should be tangential to the boundary both on entry and exit to the event. An analysis presented by Fuselier *et al.* (1986) in which the boundary was fit to a paraboloid of revolution gives a subsolar stand-off distance of *ca.* 4×10^4 km (approximately the expected subsolar shock location for the Giacobini-Zinner production rate), and a distance along the spacecraft trajectory that is approximately consistent with the *in situ* observations. Thus consistent evidence does exist for the presence of a shock in the flow surrounding Giacobini-Zinner, at least in the subsolar régime.

It should also be mentioned with regard to the mass-loaded region that effects produced by

PHILOSOPHICAL TRANSACTIONS OF THE ROYAL SOCIETY A MATHEMATICAL, PHYSICAL & ENGINEERING SCIENCES

the falling bulk speed were also observed in the alpha-particle observations made by the ion composition experiment (Ogilvie *et al.* 1986). Heavy ions observed in the inner part of the sheath region by this instrument indicate a preponderance of water-group ions (H_2O^+ with some H_3O^+), though some ions of mass *ca.* 30 (probably CO^+ or HCO^+) and *ca.* 23 (possibly Na^+ or C_2^+) were also detected.

Turning now to the central cold-plasma region, the analysis presented by Zwickl *et al.* (1986) shows a three component electron population to be present (see also Bame *et al.* 1986). The two higher-energy components have relatively constant density in this region ($T_e \approx 12$ eV with $n_e \approx 15$ cm^{-3}, and $T_e \approx 100$ eV with $n_e \approx 0.25$ cm^{-3}) and are thought to correspond to locally produced electrons resulting from photoionization of water molecules, and the solar-wind 'halo' population, respectively. If so, the presence of the 'halo' in this region indicates its accessibility to solar-wind particles, presumably by motion along 'open' tail magnetic-field lines. The main density variations in the region are then confined to the coldest population having temperatures below 3–4 eV. Because the lower energy limit of the electron spectrometer is 10 eV, determinations of the parameters of this population are of limited accuracy, leading principally to overestimates of the temperature and underestimates of the density. However, accurate values were obtained in this region from analysis of the thermal noise produced by the electrons, as detected by the radio-wave experiment (Meyer-Vernet *et al.* 1986*a*, *b*). These data show in particular that in the density spike (PT), the temperature dropped to *ca.* 1 eV while the density peaked at *ca.* 670 cm^{-3}. Zwickl *et al.* (1986) suggest that these electrons are produced by photoionization close to the nucleus, where they can become collisionally cooled by the cold neutrals before flowing outwards to the vicinity of the spacecraft.

3. Magnetic field observations

Figure 4 shows an overview of the magnetic field observations, complementary to the plasma overview shown in figure 2 (Smith *et al.* 1986). In this case, however, data for 6 h are shown, again nearly centred on closest approach. The four panels show the three field components and the field magnitude. B_x is positive towards the Sun, B_y to the east of the Sun and B_z northward. Comparison with figure 2 shows that there exists direct correspondence between magnetic and plasma features. In particular, in the mass-loaded region the mean field was compressed and draped, as expected, and extreme levels of compressional turbulence were also observed corresponding to the fluctuations in plasma properties, while within the 'intermediate coma' an induced bipolar magnetotail was observed as can be seen from the two large, oppositely directed spikes in B_x in the upper panel. The latter feature thus confirms the theoretical proposals originally made by Alfvén (1957).

At largest distances from the comet, up to *ca.* 10^6 km or more, the field data is characterized by the appearance of waves of period *ca.* 100 s (75–135 s), which are undoubtedly the counterpart of the *ca.* 2 min plasma fluctuations discussed by Gosling *et al.* (1986). Tsurutani & Smith (1986*b*) suggest that the waves are due to a resonant instability associated with heavy-ion pick up, in which the wave period in the spacecraft frame (approximately the parent neutral frame) is approximately the heavy ion gyroperiod. The predominant heavy ion at large distances is expected to be oxygen, giving a gyroperiod of *ca.* 130 s in a field of 8 nT, in approximate agreement with this suggestion. The waves are linearly polarized, generally have a compressional component, and exhibit non-sinusoidal waveforms. Some published examples

PHILOSOPHICAL TRANSACTIONS OF THE ROYAL SOCIETY A MATHEMATICAL, PHYSICAL & ENGINEERING SCIENCES

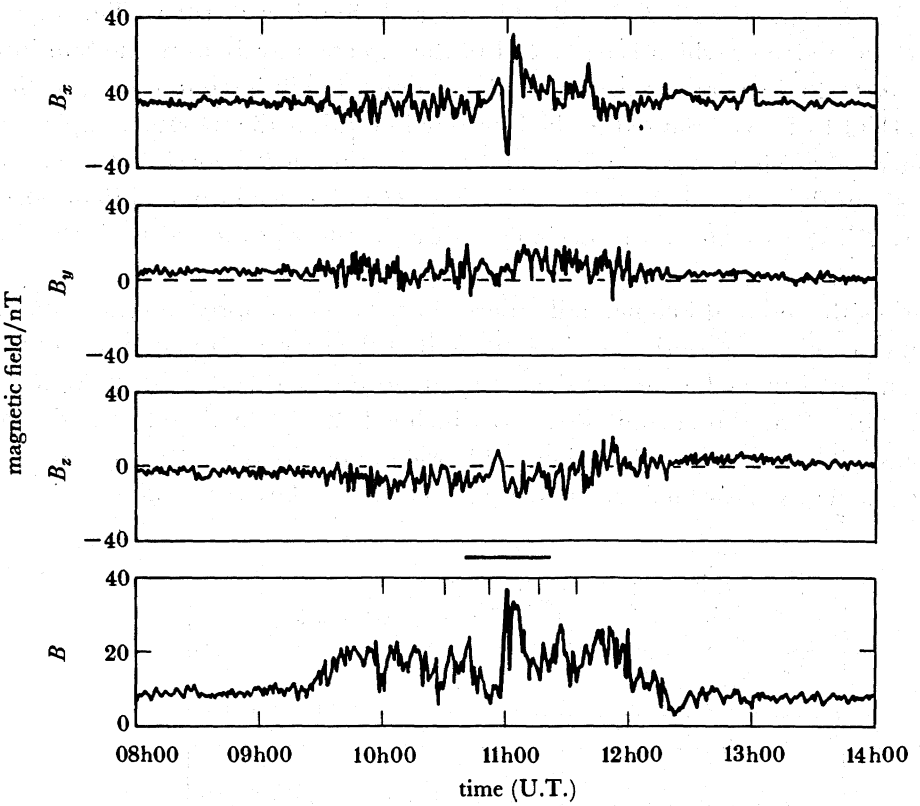

FIGURE 4. Overview of the magnetic field observations (1 min averages) at Giacobini-Zinner on 11 September 1985. Positive B_x points towards the Sun, B_y to the east of the Sun and B_z northward. B is the total field strength. (From Smith *et al.* 1986.)

(e.g. Smith *et al.* 1986; Tsurutani & Smith 1986*b*) appear to exhibit relatively slow approximately linear variations of the field components associated with increases in field strength, followed by more rapid 'returns' of the field and strength reductions. During the latter intervals discrete damped wave packets of waves of period *ca.* 3 s (1–7 s) occur, which at least visually give the impression of 'ringing' of the system resulting from the rapid change in the long-period wave. The wave packets last for *ca.* 15 s, have amplitudes 10–15 nT, and the waves are left-hand circular polarized in the spacecraft frame and propagate nearly parallel to the ambient field (Tsurutani & Smith 1986*b*).

Well away from the comet the power in the long-period magnetic waves is mainly confined to the field components transverse to the magnetic field, and this power steadily grows as the comet is approached (Tsurutani & Smith, 1986*a*). However, the power in the compressional component is strongly enhanced within the mass-loaded region, with sharp onset and termination at 09h30 and 12h20 U.T., respectively, approximately coinciding with the boundaries of the region of compressed average field (Jones *et al.* 1986). These authors have also pointed out that the locations of these boundaries are compatible with those expected for a Mach 2 shock at the Giacobini-Zinner gas production rate (similar to the conclusions of Fuselier *et al.* (1986)), and that the observed field compressions and inferred boundary orientations are not incompatible with this interpretation.

Despite the extreme levels of magnetic turbulence observed in the mass-loaded region, the

effects of field-draping are nevertheless evident in figure 4 (Smith *et al.* 1986). The main effect is seen in the B_x component, which is enhanced in the direction away from the Sun inbound (south of the comet), and reverses to become mainly sunward pointing outbound (north of the comet) up to 11h42 U.T. As discussed in the introduction, this is the signature expected for a southerly pointed solar-wind magnetic field, and examination of B_z shows that it was indeed negative throughout this interval. At 11h42 U.T., however, B_z turned from south or north and correspondingly B_x reversed in sign to become positive again, as expected from the draping picture.

The structure of the induced magnetotail observed near closest approach is also compatible with the draping picture (appropriate to $B_z < 0$), in that the spacecraft first entered the away ($B_x < 0$) lobe and then crossed a current sheet into the toward ($B_x > 0$) lobe. Examination of the field data shows that the current sheet was inclined at 45° to the ecliptic during the encounter, compatible with the solar-wind field orientation (Slavin *et al.* 1986), a result confirmed independently from analysis of energetic ion data (Daly *et al.* 1986).

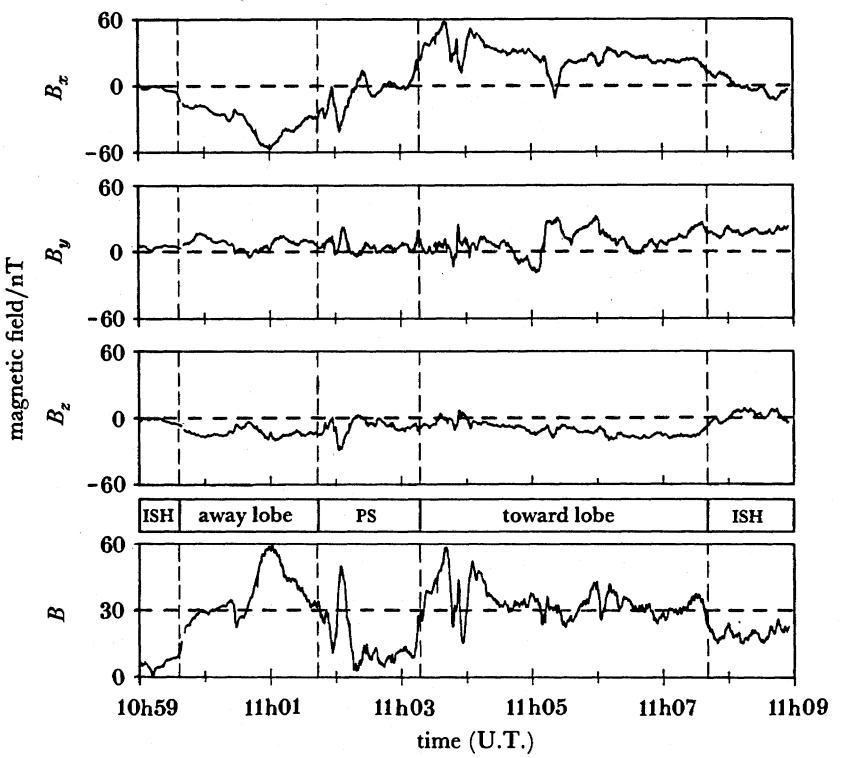

FIGURE 5. High-resolution (three vectors s^{-1}) magnetic-field data obtained during the crossing of the magnetotail. The outer vertical dashed lines mark the boundaries between the tail lobes and the 'ionosheath' (ISH), and the inner dashed lines indicate the location of the current sheet (plasma sheet, PS) region. (From Slavin *et al.* 1986.)

Details of the magnetotail data are shown in figure 5, taken from Slavin *et al.* (1986). The lobes have sharp outer boundaries of width *ca.* 200 km (outer dashed lines), which are flared in direction away from the comet–Sun axis by *ca.* 20° to 40°. Inside the boundary the field increases to *ca.* 60 nT near the edge of the plasma sheet, and then falls to *ca.* 5 nT within the latter. Small-scale field fluctuations are also present, which may be due to tail motion, though other processes may also be present (Slavin *et al.* 1986).

Comparing the magnetotail data in figure 5 with the corresponding plasma data in figure 3 it can be seen that the outbound 'away lobe' corresponds closely to the outbound 'intermediate coma' region (where the plasma density varies as r^{-2}), and that the central density spike corresponds to the plasma sheet (PS in figure 5). However, despite the approximate inbound–outbound symmetry in the 'intermediate coma' plasma data (see also Meyer-Vernet *et al.* 1986*b*), it can be seen that the inbound 'away lobe' occupies only the innermost part of the inbound 'intermediate coma' region. This leads one to suspect that the weak field region observed in the outer part of the latter is physically associated with the tail structure. The relation remains as yet unclear, though several ideas (in terms, for example, of a fragmented nucleus, gas jets, reconnected field lines) have been outlined by Smith *et al.* (1986).

Finally it should be mentioned that despite the large densities observed in the 'spike', the cold (*ca.* 1 eV) electron pressure within it is insufficient to balance the maximum lobe field pressure by approximately an order of magnitude (Smith *et al.* 1986). Because no significant pressure is associated with warm or hot electrons in this region (Meyer-Vernet *et al.* 1986*b*), the lobe pressure must be balanced by ions of temperature *ca.* 10 eV, ten times hotter than the thermal-electron component.

4. Plasma-wave observations

An overview of the plasma wave data obtained during the Giacobini-Zinner encounter is shown in figure 6, taken from Scarf *et al.* (1986). This shows the wave power against time for a set of frequency channels spanning 31–310 Hz for the magnetic field data in the lower panel, and 310 Hz to 100 kHz for the electric field data in the upper panel. Nine orders of magnitude in wave power is contained between each pair of horizontal lines, so that the vertical scales are

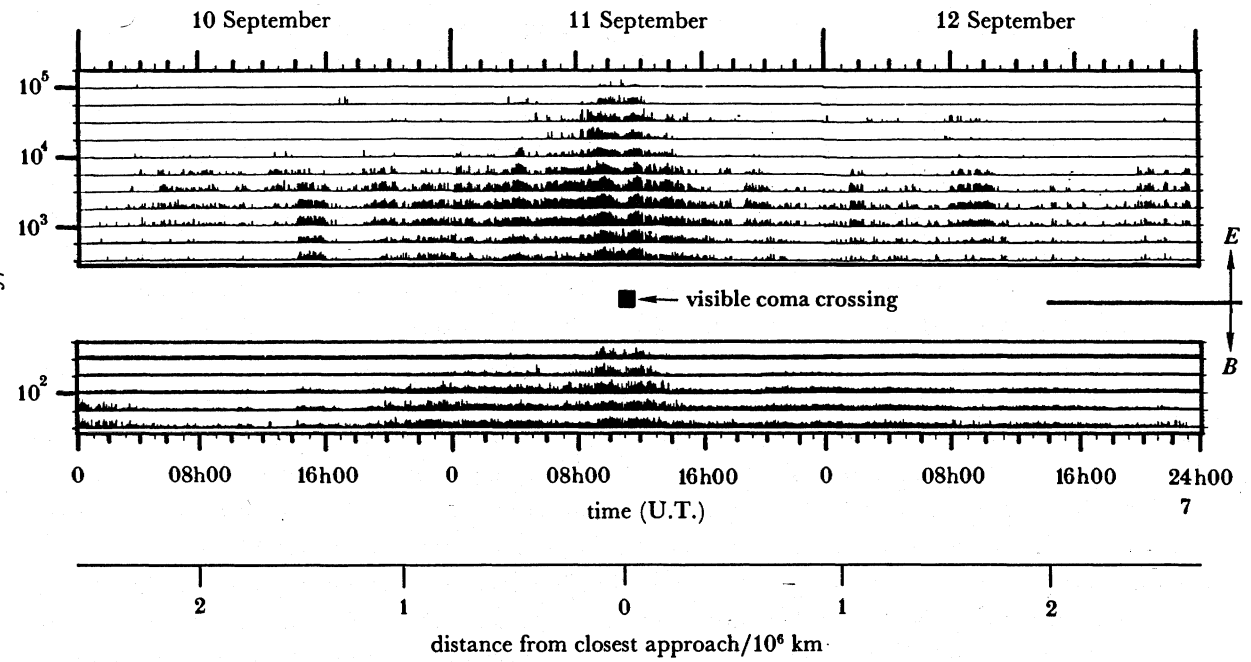

Figure 6. Overview of plasma wave observations (128 s peak amplitudes in eleven electric field channels 310 Hz–100 kHz, and five magnetic channels 31–310 Hz) for 10–12 September 1985. The amplitude scale is logarithmic with nine orders of magnitude of signal power between each pair of horizontal lines. (From Scarf *et al.* 1986.)

very compressed. Data for three days are shown, centred on closest approach, such that this scale is much larger than those used for the plasma and magnetic field overviews (figures 2 and 4). This plot therefore emphasizes the large (several million kilometres) scale of the ion pick-up region in which comet-associated waves were nearly continuously recorded.

Three principal wave types can be seen in the figure. Throughout the pick-up region, whistler-mode electromagnetic waves with frequencies less than 100 Hz, and ion-acoustic electrostatic waves with frequencies from a few 100 Hz to 10 kHz were nearly continuously present, though the latter have a more 'bursty' appearance. Like the waves of period of *ca.* 100 s observed in the plasma and magnetometer data over similar spatial scales, these waves are presumably set up by instabilities associated with the pick-up process, though theoretical details have yet to be investigated. Bursts of electron plasma oscillations at frequencies of a few tens of kilohertz can also be seen in the pick-up region nearer the comet, associated with, and presumably generated by, the electron 'heat-flux' events discussed in §2 (Fuselier *et al.* 1986).

As the comet was approached, the amplitudes of the characteristic whistler and ion-acoustic waves generally increased, but close to the comet, in the vicinity of the mass-loaded region, the character of the wave data underwent abrupt changes across thin structures that have the wave characteristics of shock traversals (Scarf *et al.* 1986). Downstream from these structures the waves are impulsive, broadband (extending to a few hundred hertz (approximately the electron gyrofrequency) in the magnetic data and to a few tens of kilohertz (approximately the electron plasma frequency) in the electric field data) and are as intense as any waves previously seen by the ICE wave instrument. Several such wave boundaries were observed inbound to the comet, between 08h27 and 09h11 U.T., which thus appear to relate to the electron 'heat flux' events rather than to the *ca.* 09h20–09h30 U.T. inbound 'bow wave' observed by other instruments (§2, 3 and 5). Outbound, however, the boundary of broadband waves occurred at 12h20 U.T., coincident with simultaneous changes recorded in the field and particle data.

In the central region of the encounter where the plasma became dominated by cold comet particles the plasma wave amplitudes were much reduced, as can just be discerned in figure 6. However, a large number of impulsive broadband signals were observed in this region due to dust grain impact (Scarf *et al.* 1986; Gurnett *et al.* 1986). These bursts were mainly observed in the interval ± 20 min about closest approach, corresponding to $\pm 2.5 \times 10^4$ km along the trajectory. Due to the south-to-north motion of the spacecraft relative to the comet, most impacts were expected on its upper surface, of area 2.4 m^2. Ground-based IR imagery then leads to expected fluxes that depend upon the assumed size of the dust grains, varying from several hundred per second for micrometre-sized grains to a few tens per second for particles of *ca.* 10–20 μm (Campins *et al.* 1986). By comparison Gurnett *et al.* (1986) report dead-time corrected fluxes peaking at *ca.* 0.5 s^{-1}. They infer that impacts on the spacecraft body were not detected by the instrument, only impacts on the antenna wire itself, whose area is a factor of *ca.* 50 less. The reason may be that the spacecraft upper surface is recessed well below the level of the solar cells surrounding the cylindrical body of the spacecraft, such that the antennas were shielded from the plasma cloud resulting from impacts on the upper surface. Even so, the observed rates suggest unexpectedly large dust-grain sizes in the range 10–20 μm. This result probably relates to the observation that meteors associated with Giacobini-Zinner (the Giacobinid or Draconid showers) are of unusually low density.

PHILOSOPHICAL TRANSACTIONS OF THE ROYAL SOCIETY A MATHEMATICAL, PHYSICAL & ENGINEERING SCIENCES

5. Energetic ion observations

In the previous sections we reviewed the effects observed by ICE in the plasma and electromagnetic field that result from mass-loading of the solar wind flow by heavy cometary ions. It will be recalled from the introduction that these ions gain considerably energy on being picked up by the solar-wind flow. The peak energy depends on the solar-wind speed and the cone angle α between the magnetic field and solar-wind velocity vectors, (1), but is typically *ca.* 4 keV u^{-1}, such that for heavy ions of the water group (O^+, OH^+, H_2O^+ or H_3O^+), energies of several tens of kiloelectronvolts are expected. ICE carried two detectors, which measured ions of these energies, and which provided complementary information on their properties. The EPAS instrument provided measurements above 65 keV (for water-group ions) in three dimensions in velocity space with a resolution of 32 s (Hynds *et al.* 1986), while the ULECA sensor was much less sensitive to heavy ions and provided two-dimensional (ecliptic-plane) measurements with reduced time resolution (Ipavich *et al.* 1986). On the other hand the ULECA energy range extends down to 35 keV, such that heavy ion bulk parameters are more easily obtained than with EPAS, and the detector also provides some information about ion mass. Ipavich *et al.* (1986) showed that the ULECA responses were consistent with the detection of singly charged heavy (more than 12 u) ions, and by comparing the ion angular anisotropies with expectations based upon the thermal electron bulk speed, deduced that the observed ion mass was 18 ± 6 u, consistent with water-group ions.

Figure 7 gives an overview of the EPAS observations, taken from Hynds *et al.* (1986). This shows fluxes in the sunward-looking sector of a telescope viewing 30° above the ecliptic plane for four energy channels: 65–95 (E_1), 95–140 (E_2), 140–205 (E_3), and 205–310 (E_4) keV. The interval 10–13 September 1985 is shown, spanning distances of several million kilometres about the comet, with closest approach being indicated by the vertical line. It can be seen that antisunward-streaming pick-up ions were indeed observed throughout this region with fluxes that generally increase as the comet is approached, as also found by Ipavich *et al.* (1986). The fluxes show considerable variability, however, and are clearly asymmetrical about closest approach with higher fluxes being observed outbound than inbound. Sanderson *et al.* (1986) have shown that these effects result from variations in the solar-wind speed and magnetic-field direction which modulate the energy gained by the pick-up ions according to (1). It is inferred that the pick-up ions are always present, but not always with sufficient energy to be detected above the 65 keV threshold of the lowest energy channel. Broadly speaking, the inbound–outbound asymmetry was due to the solar-wind speed being much lower inbound (*ca.* 350 km s^{-1} until *ca.* 05 h U.T. on 11 September) than outbound (*ca.* 500 km s^{-1}), whereas the shorter timescale variations are related to changes in the direction of the magnetic field. The latter result shows that ions in the pick-up region are not strongly pitch-angle scattered in the solar-wind rest frame, because otherwise only velocity, but not magnetic field, modulation would be present.

Figure 8 gives details of the EPAS flux measurements closer to the comet, together with ion bulk parameters deduced from angular anisotropies and ion spectra (Richardson *et al.* 1986). The vertical dashed lines at 09h27 U.T. and 12h24 U.T. mark the locations where sharp changes in ion properties take place, thus approximately coinciding with the locations of rapid changes in plasma and magnetic field properties. The upper panel shows the direction-averaged ion flux in the lowest energy channel (65–95 keV). Inside the dashed lines, fluxes vary much

PHILOSOPHICAL TRANSACTIONS OF THE ROYAL SOCIETY A MATHEMATICAL, PHYSICAL & ENGINEERING SCIENCES

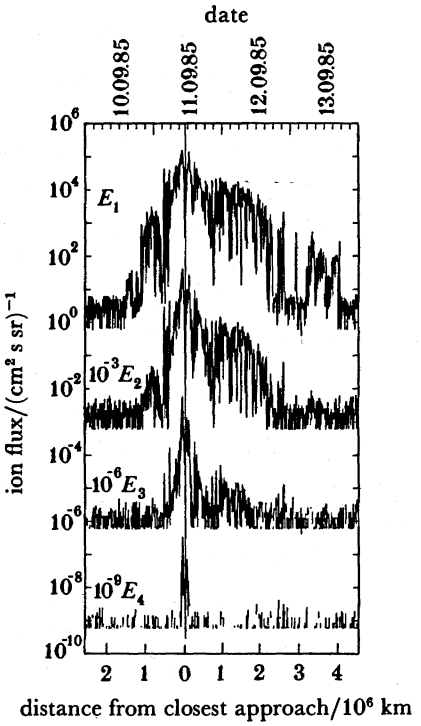

FIGURE 7. Overview of energetic ion observations by the EPAS instrument, showing the fluxes in telescope 2, inclined 30° north of the ecliptic, in sunward-pointing azimuth sector 1 against time. The four energy channels (top to bottom) correspond to water-group ions of energy 65–95, 95–140, 140–205 and 205–310 keV. The fluxes have been scaled to avoid overlap. The vertical line gives the time of closest approach. (From Hynds *et al.* 1986.)

more smoothly than outside (though with continued variability on timescales of a few minutes), and do not show strong magnetic-field modulation. This indicates that the ions have become isotropized in the plasma bulk frame in this region. Close to the comet, in the central part of the mass-loaded region, fluxes decline in strength, with a central 'slot' of *ca.* 10 min of reduced flux corresponding to the induced magnetotail structure.

The next three panels show the ion bulk speed and direction (deduced assuming that the observed ions are O^+); the dashed line shows a smoothed version of the electron bulk speed (figure 2) for comparison. The elevation angle of the flow with respect to north is represented by θ (0° to 90° indicates flow to the north, 90° to 180° flow to the south), and ϕ is the flow azimuth (180° is flow away from the Sun, 90° is flow from west to east of the Sun). These show that at the boundaries marked by the vertical lines the flow is deflected in angle away from the comet-tail axis, to the south inbound and to the north outbound, as expected from MHD models of the flow (see, for example Ip & Axford 1982 and references therein), and that the flow is also slowed by *ca.* 100 km s^{-1}. Tranquille *et al.* (1986) have examined these regions in more detail and have shown that as the plasma approaches the comet it is first deflected in elevation angle (09h24–09h28 U.T. inbound, 12h20–12h25 U.T. outbound) and then slowed (09h28–09h34 U.T. inbound, 12h14–12h20 U.T. outbound). It is the latter interval that coincides with the onset of compressional turbulence and enhanced magnitudes in the magnetic field. The full width of the transitions is *ca.* 10^4 km, corresponding to an energetic O^+ gyroradius.

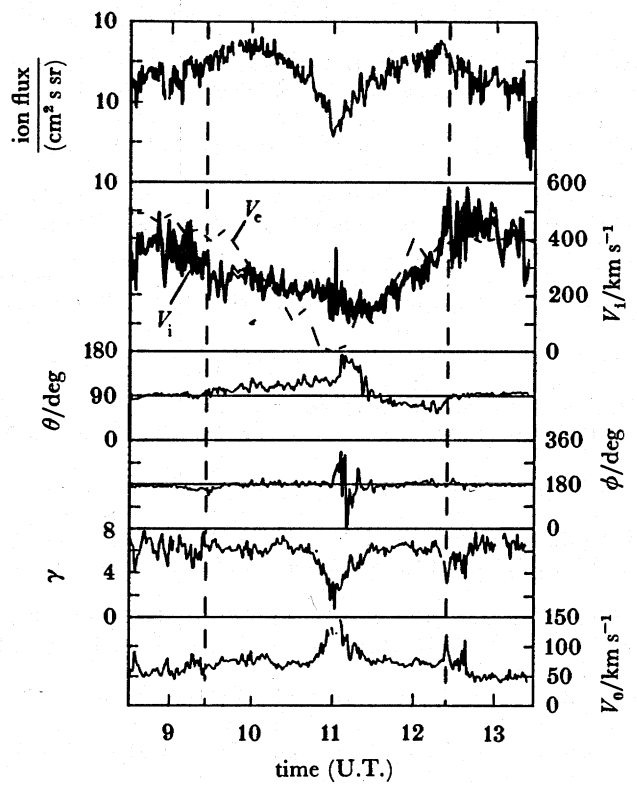

FIGURE 8. EPAS energetic ion observations and deduced ion bulk parameters for the interval 08h30 to 13h30 U.T. on 11 September 1985 spanning the mass-loaded region and induced magnetotail. The top panel shows the spin-averaged 65–95 keV ion flux, and the second to fourth panels show the deduced ion bulk speed V_i and direction (θ, ecliptic elevation, and ϕ, ecliptic azimuth), together with (dashed line) the smoothed thermal electron bulk speed V_e. The fifth and sixth panels show the power law (γ) of a fit to the spectrum of the form $dJ/dE \sim E^{-\gamma}$ and the characteristic speed V_0 of a fit of the form $f \sim \exp(-V/V_0)$ respectively. (From Richardson *et al.* 1986.)

Nearer to the comet the ions flow increasingly from north to south, and the bulk speed does not fall to very low values as indicated by the electron data. Ions are observed in this region mainly because of finite Larmor radius-penetration from the outside, such that the angular anisotropies in this region (± 30 min of closest approach) are related to density gradients rather than to plasma flows (Daly *et al.* 1986).

Finally, heavy-ion densities have been determined for the interval 06h00–16h00 U.T. from the ULECA data by Gloeckler *et al.* (1986). Their results are consistent with a water-production rate of 2.6×10^{28} mol s^{-1} and a photoionization time of *ca.* 10^6 s.

REFERENCES

Alfvén, H. 1957 *Tellus* **9**, 92–96.

Baker, D. N., Feldman, W. C., Gary, S. P., McComas, D. J. & Middleditch, J. 1986 *Geophys. Res. Lett.* **13**, 271–274.

Bame, S. J., Anderson, R. C., Asbridge, J. R., Baker, D. N., Feldman, W. C., Fuselier, S. A., Gosling, J. T., McComas, D. J., Thomsen, M. F., Young, D. T. & Zwickl, R. D. 1986 *Science, Wash.* **232**, 356–361.

Campins, H., Telesco, C. M., Decher, R., Mozurkewich, D. and Thronson, H. A. Jr 1986 *Geophys. Res. Lett.* **13**, 295–298.

Combi, M. R., Stewart, A. I. F. & Smyth, W. H. 1986 *Geophys. Res. Lett.* **13**, 385–388.

PHILOSOPHICAL TRANSACTIONS OF THE ROYAL SOCIETY A MATHEMATICAL, PHYSICAL & ENGINEERING SCIENCES

Daly, P. W., Sanderson, T. R., Wenzel, K.-P., Cowley, S. W. H., Hynds, R. J. & Smith, E. J. 1986 *Geophys. Res. Lett.* **13**, 419–422.
Fuselier, S. A., Feldman, W. C., Bame, S. J., Smith, E. J. & Scarf, F. L. 1986 *Geophys. Res. Lett.* **13**, 247–250.
Gloeckler, G., Hovestadt, D., Ipavich, F. M., Scholder, M., Klecker, B. & Galvin, A. 1986 *Geophys. Res. Lett.* **13**, 251–254.
Gosling, J. T., Asbridge, J. R., Bame, S. J., Thomsen, M. F. & Zwickl, R. D. 1986 *Geophys. Res. Lett.* **13**, 267–270.
Gurnett, D. A., Averkamp, T. F., Scarf, F. L. & Grün, E. 1986 *Geophys. Res. Lett.* **13**, 291–294.
Hynds, R. J., Cowley, S. W. H., Sanderson, T. R., Wenzel, K.-P. & van Rooijen, J. J. 1986 *Science, Wash.* **232**, 361–365.
Ip, W.-H. and Axford, W. I. 1982 In *Comets* (ed. L. L. Wilkening), pp. 588–634. University of Arizona Press.
Ipavich, F. M., Galvin, A. B., Gloeckler, G., Hovestadt, D., Klecker, B. & Scholer, M. 1986 *Science, Wash.* **232**, 366–369.
Jones, D. E., Smith, E. J., Slavin, J. A., Tsurutani, B. T., Siscoe, G. L. & Mendis, D. A. 1986 *Geophys. Res. Lett.* **13**, 243–246.
Mendis, D. A. & Houpis, H. L. F. 1982 *Rev. Geophys. Space Phys.* **20**, 885–928.
Meyer-Vernet, N., Couturier, P., Hoang, S., Perche, C., Steinberg, J. L., Fainberg, J. & Meetre, C. 1986*a* *Science, Wash.* **232**, 370–374.
Meyer-Vernet, N., Couturier, P., Hoang, S., Perche, C. & Steinberg, J. L. 1986*b* *Geophys. Res. Lett.* **13**, 279–272.
Ogilvie, K. W., Coplan, M. A., Bochsler, P. & Geiss, J. 1986 *Science, Wash.* **232** 374–377.
Richardson, I. G., Cowley, S. W. H., Hynds, R. J., Sanderson, T. R., Wenzel, K.-P. & Daly, P. W. 1986 *Geophys. Res. Lett.* **13**, 415–418.
von Rosenvinge, T. T., Brandt, J. C. & Farquhar, R. W. 1986 *Science, Wash.* **232**, 353–356.
Sanderson, T. R., Wenzel, K.-P., Daly, P. W., Cowley, S. W. H., Hynds, R. J., Smith, E. J., Bame, S. J. & Zwickl, R. D. 1986 *Geophys. Res. Lett.* **13**, 411–414.
Scarf, F. L., Coroniti, F. V., Kennel, C. F., Gurnett, D. A., Ip, W.-H. & Smith, E. J. 1986 *Science, Wash.* **232**, 377–381.
Slavin, J. A., Smith, E. J., Tsurutani, B. T., Siscoe, G. L., Jones, D. E. & Mendis, D. A. 1986 *Geophys. Res. Lett.* **13**, 283–286.
Smith, E. J., Tsurutani, B. T., Slavin, J. A., Jones, D. E., Siscoe, G. L. & Mendis, D. A. 1986 *Science, Wash.* **232**, 382–385.
Steinberg, J. L., Fainberg, J., Meyer-Vernet, N. & Hoang, S. 1986 *Geophys. Res. Lett.* **13**, 407–410.
Strauss, M. A., McCarthy, P. J. & Spinrad, H. 1986 *Geophys. Res. Lett.* **13**, 389–392.
Thomsen, M. F., Bame, S. J., Feldman, W. C., Gosling, J. T., McComas, D. J. & Young, D. T. 1986 *Geophys. Res. Lett.* **13**, 393–396.
Tranquille, C., Richardson, I. G., Cowley, S. W. H., Sanderson, T. R., Wenzel, K.-P. & Hynds, R. J. 1986 *Geophys. Res. Lett.* **13**, 853–856.
Tsurutani, B. T. & Smith, E. J. 1986*a* *Geophys. Res. Lett.* **13**, 259–262.
Tsurutani, B. T. & Smith, E. J. 1986*b* *Geophys. Res. Lett.* **13**, 263–266.
Zwickl, R. D., Baker, D. N., Bame, S. J., Feldman, W. C., Fuselier, S. A., Huebner, W. F., McComas, D. J. & Young, D. T. 1986 *Geophys. Res. Lett.* **13**, 401–404.

PHILOSOPHICAL TRANSACTIONS OF THE ROYAL SOCIETY A MATHEMATICAL, PHYSICAL & ENGINEERING SCIENCES